Journal of Crystal Growth 363 (2013) 40–43

Contents lists available at SciVerse ScienceDirect

Journal of Crystal Growth

journal homepage: www.elsevier.com/locate/jcrysgro

Epitaxial growth of InGaAs on $MgAl_2O_4$ spinel for one-sun photovoltaics

W.L. Rance, A.G. Norman, A.J. Ptak*

National Renewable Energy Laboratory, 15013 Denver West Parkway, Golden, CO 80401, United States

ARTICLE INFO

Article history:
Received 23 April 2012
Received in revised form
6 September 2012
Accepted 21 September 2012
Communicated by: H. Asahi
Available online 28 September 2012

Keywords:
A1. Planar defects
A1. Substrates
A3. Molecular beam epitaxy
B2. Semiconducting III–V materials
B3. Solar cells

ABSTRACT

We demonstrate coincident-site lattice-matched growth of InGaAs layers on (001) $MgAl_2O_4$ spinel substrates, using a 45° rotation between the lattices, by molecular beam epitaxy. This is the first step towards easily removable multijunction solar cells with inert, reusable substrates. High-resolution cross-sectional transmission electron microscopy (TEM) measurements indicate that microtwins originate at the InGaAs/spinel interface, but tend to annihilate leaving the upper parts of layers relatively twin-free . Plan-view TEM indicates a high density of threading dislocations. InGaAs layers grown at elevated temperatures show improved transport properties, with majority-carrier mobilities approaching typical values for homoepitaxial GaAs on GaAs substrates. Simple *p–i–n* junctions show photovoltaic efficiencies above 1%.

© 2012 Elsevier B.V. All rights reserved.

Multijunction III–V photovoltaics (PV) have, by far, the highest solar conversion efficiencies of any solar technology. To reach higher efficiencies, it is necessary to shift the lattice constant of III–V materials away from those available in nature to those where available bandgaps more closely match the solar resource [1–6]. This is typically achieved with thick, graded-lattice-constant buffer layers that add time, material, and cost to traditional III–V multijunction solar cells. The lattice-mismatched approaches can also increase defect levels (typically in the form of threading dislocations) enough to severely limit the power conversion efficiency [7]. An alternate approach is to move away from the standard Ge and GaAs substrates used in multijunction PV and use a substrate that enables lattice-matched III–V materials with greater overlap with the solar spectrum [8]. For example, moving to somewhat larger lattice constants from GaAs opens up a wider range of direct bandgap III–V alloys than is available lattice-matched to GaAs and Ge. The (Al, Ga, In)(As, P) family of materials spans a direct bandgap range of ~1.2–2.2 eV at a lattice constant of ~5.71 Å, providing the opportunity for high-efficiency, lattice-matched multijunction III–V solar cells. Unfortunately, no readily available material exists with this lattice constant for use as a substrate. However, for (001) oriented face-centered cubic (fcc) crystals, a coincident-site lattice-matched condition is met when an epilayer has a lattice parameter a factor of $\sqrt{2}$ larger or smaller than the substrate, and that layer is rotated 45° about the [001] axis relative to the substrate [9]. In the specific case of the III–V alloy $In_{0.15}Ga_{0.85}As$, with a lattice spacing of 5.71 Å, the coincident-site lattice-matched condition is met for fcc materials with a lattice parameter of either 8.08 Å or 4.04 Å, as shown in the inset of Fig. 1. $MgAl_2O_4$ spinel is a commercially-available crystal with a lattice parameter of 8.08 Å, and an oxygen fcc sublattice spacing of 4.04 Å, making it an ideal substrate for III–V PV at the 5.71 Å lattice constant. Spinel is also inert to most chemicals, so substrate liftoff can be accomplished without the need to repolish the substrate or replace any removed material. This is important because repolishing GaAs substrates is economically unfeasible for one-sun applications, where the substrate represents a significant fraction of the final cost of a module. Spinel is a very hard material and should avoid known issues with thermally-induced slip-lines in reused GaAs substrates. Spinel is also of great interest as a final "lattice matched" oxide buffer layer for the growth of III–V solar cells or other devices on cheap metal templates such as ion-beam assisted deposition (IBAD) textured MgO on Ni foil [10] or on rolling-assisted biaxially textured substrates (RABiTS) such as Ni-W [11,12]. The 45° rotation was previously observed for GaAs grown on (001) spinel, despite the 1% lattice mismatch [13]. Realization of lattice-matched InGaAs on spinel has the obvious advantage of reduced or eliminated concentrations of extended crystal defects compared to the mismatched GaAs/spinel case. Here, we demonstrate this coincident-site lattice-matched condition for the heteroepitaxy of InGaAs on spinel as the first step toward multijunction, lattice-matched III–Vs with substrate reuse, and report the overall quality of InGaAs layers as determined by X-ray diffraction (XRD), electron back-scatter diffraction (EBSD), and transmission electron microscopy (TEM). The optoelectronic properties are also described from Hall measurements, photoluminescence spectra, and preliminary photovoltaic devices.

* Corresponding author. Tel.: +1 303 384 6660; fax: +1 303 384 6430.
E-mail address: aaron.ptak@nrel.gov (A.J. Ptak).

0022-0248/$ - see front matter © 2012 Elsevier B.V. All rights reserved.
http://dx.doi.org/10.1016/j.jcrysgro.2012.09.037

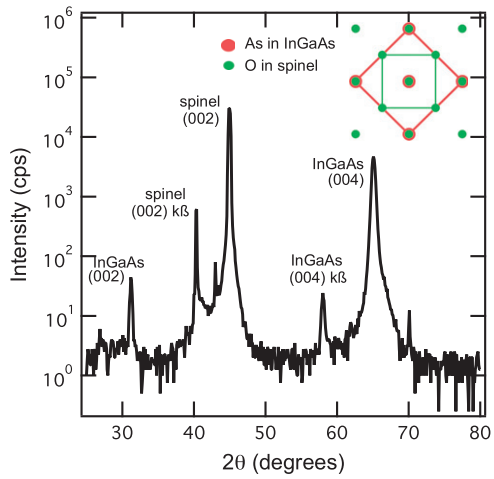

Fig. 1. XRD ω-2θ measurement of the (004) planes of a 1-μm-thick InGaAs/spinel film. A schematic representation of the coincident-site lattice-matched condition for InGaAs growth on spinel is shown in the inset.

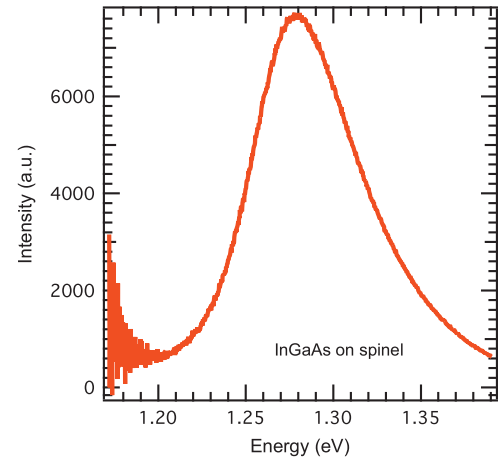

Fig. 2. Room temperature PL spectrum of InGaAs grown coincident-site lattice-matched on (001) spinel.

To determine the efficacy of this coincident-site approach, InGaAs layers and devices were grown on (001) oriented $MgAl_2O_4$ spinel by solid-source molecular beam epitaxy (MBE) at a growth rate of 1 μm/hr. Standard effusion cells for Ga and In, and a cracker cell that converted As_4 to As_2 were used. The transparent spinel substrates were loaded into the system in In-free holders with Si backing wafers that absorbed and transferred the heat. A substrate dial temperature (T_{sub}) of 800 °C was used for all growths, except those used for Hall measurements, which had variable temperature. The InGaAs crystal structure and surface orientation were investigated by XRD and EBSD. XRD ω-2θ scans were measured using a Rigaku Ultima IV X-ray diffractometer, and EBSD analysis was performed using a HKL Nordlys detector mounted in a Hitachi S-3400N scanning electron microscope. Composition and epilayer thicknesses were confirmed by modeling the dielectric function and refractive index obtained from spectral ellipsometry. The InGaAs/spinel interface and InGaAs layer microstructure were studied with TEM. The electronic properties were measured using Hall effect measurements with annealed Au/Sn/Au (*n*-type) or Au/Zn/Au (*p*-type) contacts in a Van der Pauw configuration. Photoluminescence spectra were acquired at room temperature using the 632.8 nm line of a He–Ne laser as an excitation source. For solar cells, Au/Sn/Au and Au contacts were electroplated on the emitter and back contact layer, respectively.

Fig. 1 shows a symmetric XRD measurement of a 1-μm-thick InGaAs layer grown on spinel. The (004) diffraction peaks generated by both Cu kα and kβ radiation are present for both the spinel and InGaAs. No other diffraction peaks exist indicating the InGaAs layer is single domain and (001) oriented. The inclusion of both the Cu kα and kβ peaks complicates the spectrum but the additional available intensity allows one to see that the material is indeed single-phase . The position of the InGaAs (004) diffraction peak yields a lattice parameter and In composition for this sample of 5.72 Å and 0.16, respectively, assuming that the material is fully strained to the substrate. If, however, we assume that the layer is completely relaxed, the In composition may be much higher. It is difficult to directly determine the extent of relaxation from asymmetric XRD measurements or reciprocal space maps in this case because the peaks are very widely separated and fairly broad. The errors introduced by this method are on the order of the difference between relaxed and strained epilayers. As we will show from TEM measurements below, there is a significant density of extended defects in these layers. Spectral ellipsometry was used to measure the bandedge from the dielectric function and confirms an In composition of 16% for these layers. In addition, Fig. 2 shows a room temperature photoluminescence measurement of the InGaAs layer indicating a broad but strong emission from what is presumed to be the bandedge region near ~1.28 eV, which correlates with an In composition closer to 10%. It is possible that there is In-related phase separation occurring in these layers, which would help to explain these different results and the substantial width of the XRD peak.

EBSD of both the InGaAs and a portion of the substrate that was masked during growth were used to determine the surface quality and orientation of InGaAs relative to the spinel. The (111) pole figures of the InGaAs and spinel, shown in Fig. 3, confirm the existence of the coincident-site lattice-matched condition described above. That is, the InGaAs lattice is rotated by 45° with respect to the substrate. These pole figures represent a compilation of typically several thousand measurements of crystal orientation. Even though the composition for this sample is slightly above the optimum value of $x=0.15$, the low orientation variation of the InGaAs poles (represented by the tight grouping of the thousands of data points in Fig. 3) compared to the spinel also indicates the (001) oriented InGaAs layer has good quality.

High-resolution TEM images of the InGaAs/spinel interface show the existence of a high density of microtwins in the InGaAs layers, Fig. 4. While the InGaAs/spinel interface is abrupt, the substrate displays nanometer-scale roughness that may contribute to the nucleation of twin defects. Indeed, polishing scratches are visible on the surface of the substrates in an optical microscope before growth. Attempts to remove the scratches prior to growth, including polishing, wet chemical etching, and high-temperature annealing in air, oxygen, and vacuum, were not successful. The microtwins visible in the TEM image are associated with the {111} InGaAs planes and a high density are observed to originate at the InGaAs/spinel interface, although large areas of twin-free material are commonly observed further away from the interface. This suggests that twins and other crystalline defects annihilate or self-heal during growth. Plan-view TEM, Fig. 5, indicates a high density, $>10^9\,cm^{-2}$, of threading dislocations is also present in the InGaAs layers in addition to the twins. These may be associated with the initial nucleation of the InGaAs on the rough spinel substrate or the slight lattice mismatch that is present.

Fig. 6(a) shows the results of Hall effect measurements on 1-μm-thick Si-doped InGaAs layers. The Si doping level is constant in these samples, verified by secondary-ion mass spectrometry ($[Si]\sim 8–9\times 10^{17}\,cm^{-3}$). Significant compensation of the Si donors occurs at low substrate temperatures, although a clear improvement in both dopant activation and electron mobility is

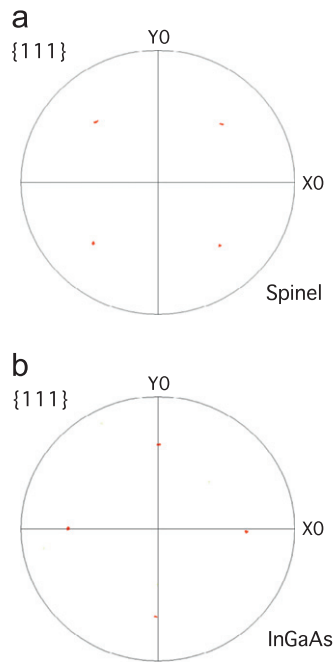

Fig. 3. (111) EBSD pole figures of (a) the spinel substrate and (b) InGaAs layer surfaces.

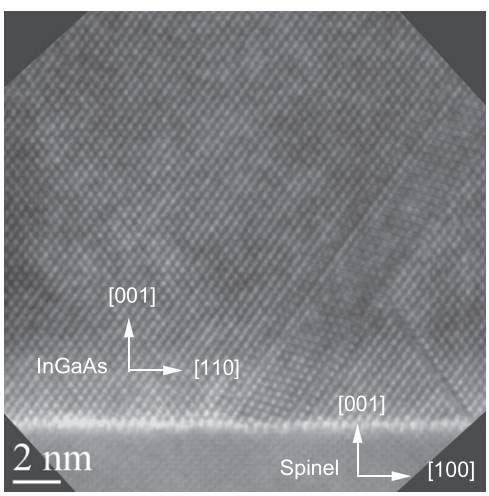

Fig. 4. High-resolution cross-section TEM image of the InGaAs/spinel interface showing microtwins generated on {111} InGaAs planes.

evident with increased growth temperatures, likely due to improved crystal quality and a reduction in defects. In particular, the electron mobility of 775 $cm^2/V\,s$ at $T_{sub}\sim 800$ °C (dial) is within a factor of three of the expected GaAs mobility for the same doping concentration. Above 750–800 °C (dial), both the carrier concentration and mobility begin to fall, possibly correlated with increased In-related phase separation at these temperatures. Epilayers grown above this dial temperature tend to be rough and appear hazy to the eye. This may help explain the discrepancy in In composition determination between spectral ellipsometry, PL, and XRD. A similar improvement in carrier concentration and mobility with increasing substrate temperature is observed for Be-doped *p*-type samples Fig. 6(b) with hole mobilities $>20\,cm^2/V\,s$ for InGaAs layers grown at $T_{sub}\sim 800$ °C (dial) with Be concentrations in the mid-$10^{18}\,cm^{-3}$ range. This is also within a factor of 3–4 of high-quality *p*-type GaAs. The carrier mobilities are likely limited by the high density of threading dislocations and microtwins present in the layers.

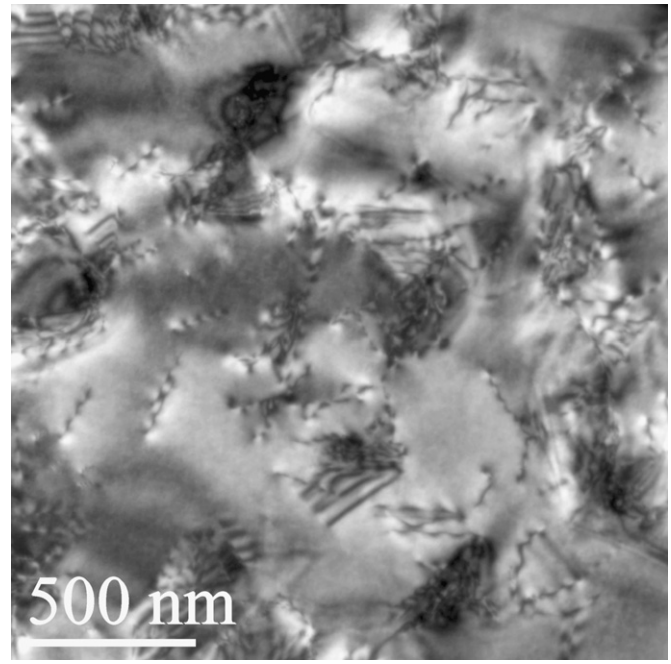

Fig. 5. 220 dark field plan-view TEM image showing high density of threading dislocations in an InGaAs layer grown on (001) spinel.

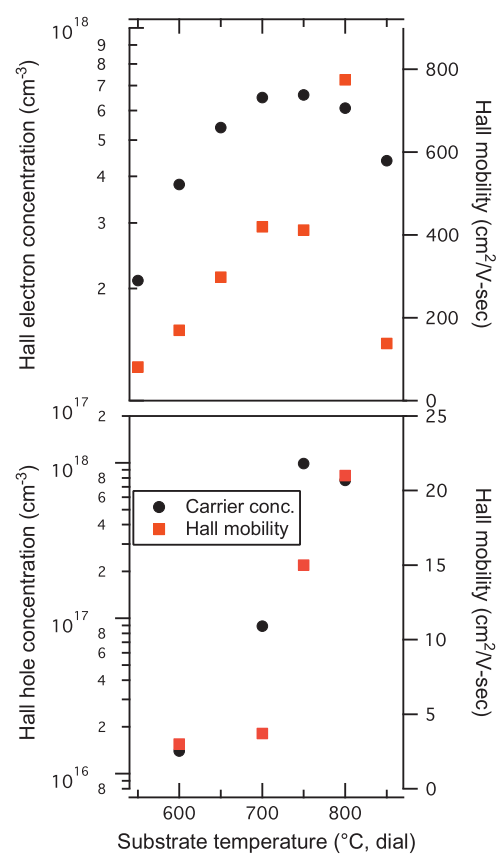

Fig. 6. Electron and hole carrier concentration (circles) and mobility (squares) for InGaAs with constant Si or Be doping versus the substrate growth temperature.

A simple *p–i–n* structure was grown at $T_{sub}\sim 800$ °C (dial), and solar cells with a device area of 0.05 cm^2 were processed using standard photolithography techniques, with the device structure outlined in the inset of Fig. 7. Due to the insulating nature of spinel, an additional wet chemical etch was required to expose

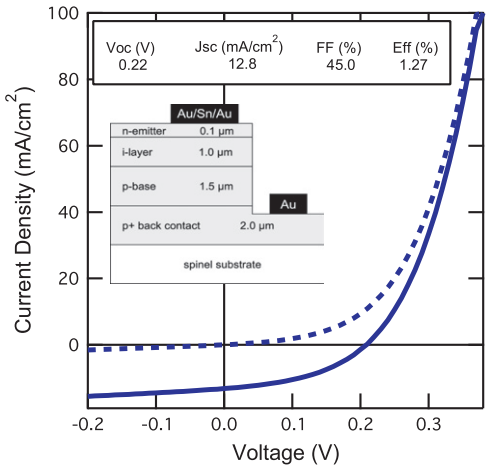

Fig. 7. IV curves of an InGaAs *p–i–n* junction in the light under AM1.5D (solid line) and dark (dashed line). Inset: schematic of the device structure.

the back contact layer prior to electroplating. Fig. 7 shows the light and dark IV measurements performed under an approximated AM1.5D solar spectrum. These initial InGaAs/spinel devices displayed power conversion efficiencies of 1.3%, despite the high level of threading dislocations and twin defects and the fact that no window layer or back-surface field (BSF) was used in this preliminary device. The short-circuit current (J_{SC}) of 13 mA/cm^2 is reasonable, but the open-circuit voltage (V_{OC}) of 0.22 V is quite low for a bandgap of $\sim$1.2 eV. The V_{OC} is expected to improve with better InGaAs film quality and better ohmic contacts, and improved crystal quality will likely also improve the low fill factor of 45%, which is limited due to the high series and low shunt resistance exhibited in this device.

In conclusion, we have demonstrated InGaAs grown by MBE on (001) spinel utilizing a coincident-site lattice-matched condition. InGaAs layers are single crystal and the lattice is rotated 45° relative to the spinel lattice. Spinel substrates offer a better match to the solar spectrum for direct bandgap III–V materials and the possibility of chemical removal of III–V devices with no repolishing of the substrate necessary. A high density of structural defects originating at the InGaAs/spinel interface are present, but Hall mobilities within a factor of three of values expected for homoepitaxial GaAs are demonstrated for *n*- and *p*-type InGaAs layers and room temperature photoluminescence is observed. Power conversion efficiencies were above 1% for a basic *p–i–n* device, which should be greatly improved with further material optimization, better contacts, and the use of window and BSF layers.

Acknowledgments

We thank D.L. Young for valuable conversations and technical monitoring, Sukgeun Choi for the ellipsometry data, and P. Dippo for the photoluminescence data. This work was supported by the U.S. Department of Energy under Contract no. DE-AC36-08-GO28308 with the National Renewable Energy Laboratory.

References

[1] F. Dimroth, R. Beckett, M. Meusel, U. Schubert, A.W. Bett, Progress in Photovoltaics: Research and Applications 9 (2001) 362.
[2] M.W. Wanlass, S.P. Ahrenkiel, R.K. Ahrenkiel, D.S. Albin, J.J. Carapella, A. Duda, J.F. Geisz, S. Kurtz, T. Moriarty, R.J. Wehrer, and B. Werrnsman, Proceedings of the 31st IEEE Photovoltaic Specialists Conference, Orlando Florida IEEE, New York, 2005, p. 530.
[3] R.R. King, D.C. Law, K.M. Edmondson, C.M. Fetzer, G.S. Kinsey, H. Yoon, R.A. Sherif, N.H. Karam, Applied Physics Letters 90 (2007) 183516.
[4] M. Stan, D. Aiken, B. Cho, A. Cornfeld, J. Diaz, V. Ley, A. Korostyshevsky, P. Patel, P. Sharps, T. Varghese, Journal of Crystal Growth 310 (2008) 5204.
[5] J.F. Geisz, D.J. Friedman, J.S. Ward, A. Duda, W.J. Olavarria, T.E. Moriarty, J.T. Kiehl, M.J. Romero, A.G. Norman, K.M. Jones, Applied Physics Letters 93 (2008) 123505.
[6] W. Guter, J. Schone, S.P. Philipps, M. Steiner, G. Siefer, A. Wekkeli, E. Welser, E. Oliva, A.W. Bett, F. Dimroth, Applied Physics Letters 94 (2009) 223504.
[7] M. Yamaguchi, Journal of Materials Research 6 (1991) 376.
[8] E.C. Warmann, M.S. Leite, H.A. Atwater, Proceedings of the 37th IEEE Photovoltaic Specialists Conference, Seattle Washington, 2011.
[9] C.J. Palmstrom, Annual Review of Materials Science 25 (1995) 389.
[10] V. Selvamanickam, S. Sambandam, A. Sunderam, S. Lee, A. Rar, X. Xiong, A. Alemu, C. Boney, A. Freundlich, Journal of Crystal Growth 311 (2009) 4533.
[11] C.W. Teplin, M. Parans Paranthaman, T.R. Fanning, K. Alberi, L. Heatherly, S.-H. Wee, K. Kim, F.A. List, J. Pineau, J. Borstein, K. Bowers, D.F. Lee, C. Cantoni, S. Hane, P. Schroeter, D.L. Young, E. Iwaniczko, K.M. Jones, H.M. Branz, Energy and Environmental Science 4 (2011) 3346.
[12] S.H. Wee, C. Cantoni, T.R. Fanning, C.W. Teplin, D.F. Bogorin, J. Bornstein, K. Bowers, P. Schroeter, F. Hasoon, H.M. Branz, M. Parans Paranthaman, A. Goyal, Energy and Environmental Science 5 (2012) 6052.
[13] S. Maruyama, Japanese Journal of Applied Physics 24 (1985) 363.